

Cite this: *Soft Matter*, 2012, **8**, 5256

www.rsc.org/softmatter

PAPER

Oscillatory normal forces of magnetorheological fluids†

Xinglong Gong,* Chaoyang Guo, Shouhu Xuan, Taixiang Liu, Luhang Zong and Chao Peng

Received 16th February 2012, Accepted 2nd March 2012

DOI: 10.1039/c2sm25341k

The normal forces of magnetorheological fluids were investigated by a commercial magneto-rheometer with plate–plate geometry. Based on the analysis, it was found that the oscillatory normal forces can be achieved both under steady shear and oscillatory shear. The oscillatory normal forces obtained under steady shear developed from the nonparallelism of the testing plates, while the oscillatory normal forces under oscillatory shear mainly arose from the microstructure revolution of magnetorheological fluids. Finally, a dynamic simulation was utilized to analyze this oscillatory shear normal force and the formation mechanism was discussed.

1. Introduction

As a kind of smart material, magnetorheological (MR) fluids have been extensively studied during the past decades as their rheological properties could be changed quickly and reversibly under a magnetic field. Various high performance MR fluids were developed, and MR fluids have been applied in clutches, brakes, damping devices, actuators, hydraulic valves, polishing and robotic controlling systems.^{1–6} Apart from the shear properties such as viscosity and shear stress, the normal force behaviors of the MR fluid have attracted considerable attention, not only for academic interest, to understand the MR fluids, but also for the benefit in designing precision MR devices.^{6–14}

Vicente *et al.* have done the pioneer experimental research and found that the normal force could be generated only when the MR fluid was under shearing and the magnetic field reached a critical value.⁷ However, Shkel and Klingenberg theoretically indicated the static normal stress (σ_{33}) can be yielded as soon as the magnetic field was applied and the relationship can be expressed as $\sigma_{33} \propto H^2$.⁸ Afterwards, See and Tanner and Laun *et al.* presented that the non-negligible normal force was generated even when the MR Fluid was not subject to any deformation.^{9,10} Then, López-López *et al.* took the inhomogeneity of the applied field into account and explained the disagreement between these works.¹¹ In addition, Chan *et al.* showed that the static normal force could be increased by imposing shear actions on the excited MR fluid.¹² Jiang *et al.* demonstrated that the normal stress increased considerably, then decreased suddenly and significantly upon the onset of shear thickening in MR fluids.¹³ However, all these works were studied under stationary

or steady shear and the obtained normal forces were steady values and independent to the testing time.

In this work, the normal forces of MR fluids under steady shear and oscillatory shear were studied and compared by using a commercial magneto-rheometer with plate–plate geometry. The oscillatory normal forces were generated under both steady shear and oscillatory shear. The origins of the oscillatory normal forces were analyzed. At last, both theoretical modelling and dynamic simulation were undertaken to analyze the oscillatory normal forces.

2. Experimental

2.1 Materials

MR fluids were composed of carbonyl iron powder particles (CN, BASF, Germany, chemical composition (wt%): >99.5% Fe, <0.04% C, <0.01% N, 0.2% O; the average particle size was about 6 μm) in silicone oil (H201, Sinopharm Chemical Reagent Co. Ltd, China and the viscosity was about 20 mPa·s) and were prepared with a iron particle volume fraction of 30%. 2 wt% stearic acid was added to improve sedimentary stability. The samples were vigorously shaken to ensure homogeneity before measurements.

2.2 Testing technology

The plate–plate magneto-rheometer (Physica MCR301, Anton Paar, Austria) was used to measure the normal force of the MR fluids with a sensor built into the air bearing. The diameter of the plate used was 20mm and the gap between them was fixed at 1 mm. The normal forces under steady shear with time could be acquired from the system software package. However, the normal forces under oscillatory shear with time were obtained from the rheometer output with the aid of a dynamic signal analyzer (SignalCalc ACE, Data Physics, USA),¹⁴ as shown in Fig. 1. The testing temperature was set at 25 °C.

Department of Modern Mechanics, CAS Key Laboratory of Mechanical Behavior and Design of Materials, University of Science and Technology of China, Hefei, 230027, China. E-mail: gongxl@ustc.edu.cn; Fax: +86-551-3600419; Tel: +86-551-3600419

† Electronic supplementary information (ESI) available. See DOI: 10.1039/c2sm25341k

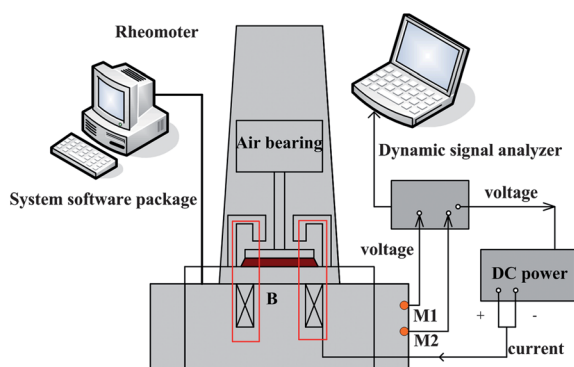


Fig. 1 Schematic of the measuring system.

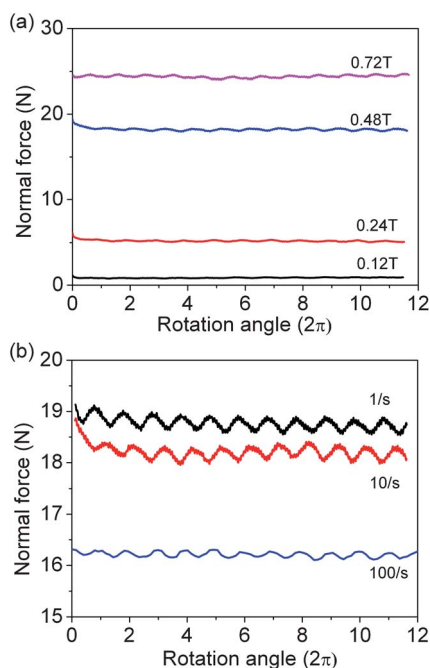


Fig. 2 Experimental normal forces of the MR fluid under steady shear (a) at 10 s^{-1} but with different magnetic fields and (b) at 0.48 T but with different shear rates.

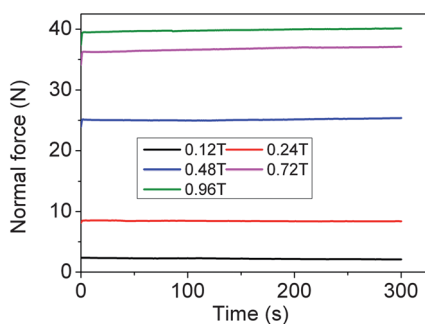


Fig. 3 Normal forces while stationary with time after applying the magnetic field.

Two types of experiments were performed to study the normal force: steady shear and oscillatory shear. In all cases, the samples were sheared without a magnetic field at 50 s^{-1} for 150 s to ensure

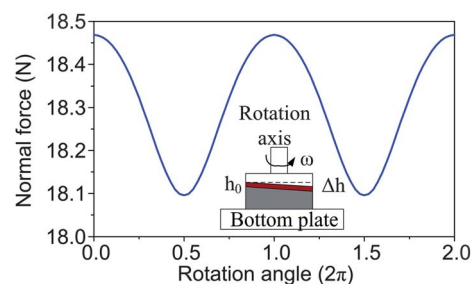


Fig. 4 Model fitting for the normal forces of the MR fluid under steady shear at 0.48 T (The inset is a schematic of the titled axis plate-plate rheometer).

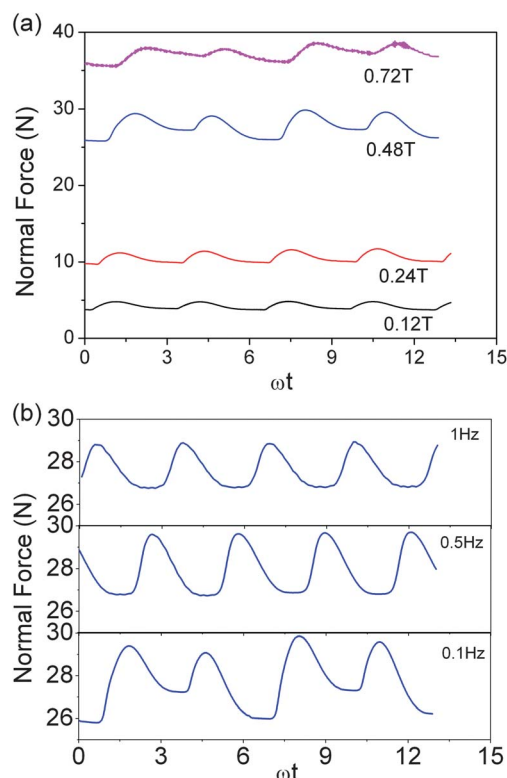


Fig. 5 Experimental normal forces of the MR fluid under oscillatory shear (a) at 0.1 Hz and different magnetic field and (b) at 0.48 T and various frequencies.

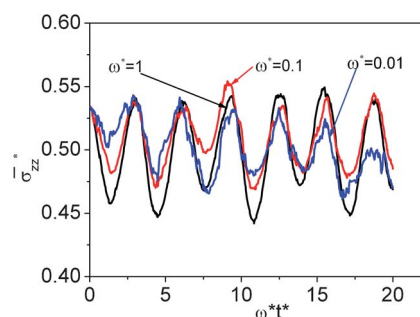


Fig. 6 Dimensionless normal stress of MR fluid under oscillatory shear calculated by dynamic simulation method.

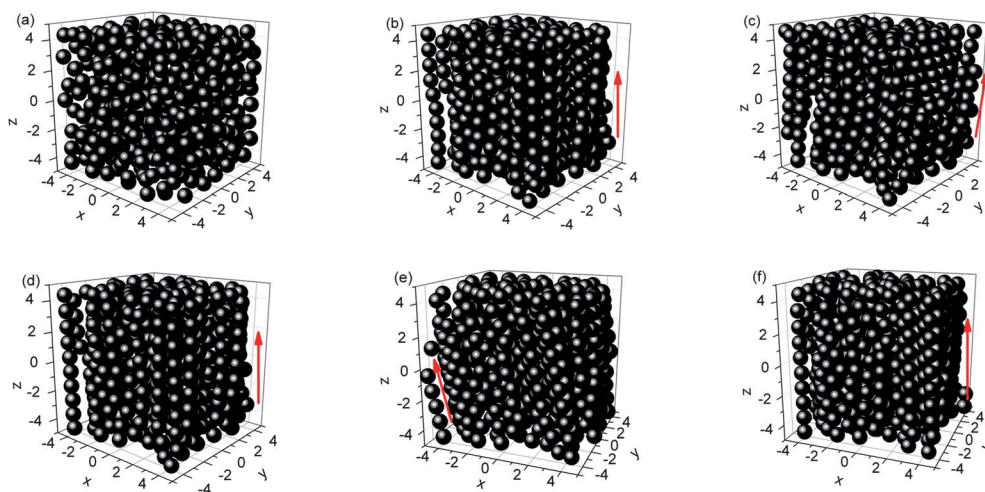


Fig. 7 Microstructure revolution of MF fluid under oscillatory shear ($\gamma_0 = 10\%$, $\omega^* = 1$); (a) initial randomly dispersed particle; (b) steady structure after certain steps where no oscillatory shear is applied and it is also the beginning structure under oscillatory shear; (c) structure after 1/4 cycle; (d) structure after 1/2 cycle; (e) structure after 3/4 cycle; (f) structure after 1 cycle.

good dispersion. Then, the shearing was stopped and the magnetic field was applied for 30 s to form a steady structure. At last the normal forces under steady and oscillatory shear were measured.

3. Results and discussion

3.1 Oscillatory normal force under steady shear

The normal forces of the MR fluid under steady shear were measured with time and magnetic fields at a shear rate of 10 s^{-1} (Fig. 2 (a)). When the magnetic field is applied, the dynamic normal forces generate and increase with an increase in the magnetic field. It should be noticed that a critical magnetic field existed during the generation of the normal forces and the value is between 20–30 mT. When the magnetic field is smaller than the critical value, the normal force is negative and very small. As soon as the magnetic field exceeds the critical value, the normal forces will change from a negative to a positive value (Fig. S1, ESI†). Fig. 2(a) shows the normal forces of the MR fluid under steady shear of 10 s^{-1} , it is very interesting to find that the dynamic normal force shows an oscillation nature. They have a period of 2π which is the same with the rotation of the rheometer axis. The oscillatory normal force is highly dependent on the magnetic field and a larger magnetic field will lead to a more obvious oscillatory nature. Moreover, with increasing of the shear rate, the normal forces decrease (Fig. 2 (b)). Similar to the above observation, the normal forces also oscillate periodically with the rotation under the constant magnetic field.

To investigate the influence of the volume fractions of the MR fluids, 10%, 20%, 40% iron based MR fluids were prepared. Similar to the 30% sample, oscillatory normal forces with a period of 2π were found for these samples. With the increased concentration, the sinusoidal phenomenon of the normal force became more obvious (Fig. S2, ESI†). During the above experiments, the gap between the testing plates was kept at 1mm. To fully understand the influence of the testing conditions on the normal forces, other gaps (0.3mm, 0.5mm and 0.8mm) have been

measured for the 30% MR fluid. It is found that the gap distance has little effect on the result (Fig. S3†). The oscillatory normal force with a period of 2π could be observed at all these gap distances and the peak–peak oscillatory normal force at 0.3mm was a little bigger than that at 0.5 mm and 0.8mm. In this work, the direction of the externally applied magnetic field was also switched by reversing the current direction through the coils. Similar to the non-reversible magnetic field, the positive normal forces of the 30% MR fluid was generated after applying the magnetic field (Fig. S4†). The oscillatory normal forces were also produced by inverting the magnetic field. This result indicated that the oscillatory normal force did not depend on the direction of the field. Based on the above analysis, the gap distance, particle concentration, direction of magnetic field are not affecting parameters for the oscillatory normal force of MR fluid under steady shear.

For the 30% MR fluid, the peak–peak amplitude of the oscillation normal forces is about 0.4 N (2% of the total normal forces). The normal force is measured with a sensor built into the air bearing with an accuracy of 0.03 N. Thus the oscillatory value would not be due to measurement error. Here, the normal force when stationary keeps constant with time for a given magnetic field (Fig. 3). Considering that the plates were parallel, López-López *et al.* pointed out that the normal force under steady shear should be a constant value and independent on the rotation of rheometer axis.¹¹ Therefore, the oscillatory normal forces must arise from the rotation of the axis.^{15–17} To this end, misalignment of the plates (the gaps are not precisely perpendicular to the rotation axis, but tilted by an angle α) leads to oscillation of the normal force.

Orellana *et al.* found the shear stress and normal force of giant electrorheological fluid also showed a oscillatory characteristic.¹⁵ It was thought that the shear stress oscillations were associated with a narrow shear band, which was a characteristic feature of granular material. This analysis could be also used to explain the oscillation of the normal force of MR fluid. Tian *et al.* tested the apparent normal stress N_d of MR fluid with the shear rate $\dot{\gamma}$ and an equation $N_d = N_{ds} + K\dot{\gamma}$ was used to fit the data, where N_{ds}

was the static N_d and K was a viscosity parameter which was negative.¹³ This is similar to the Bingham plastic model for the shear stress. As shown in Fig. 4, the upper plate moves with fixed angular speed ω set by the rheometer tool and the bottom plate remains stationary. The two plates rotate in and out of alignment with period 2π in their relative azimuthal angle φ . A shear band (fluid-like region) exists right underneath the upper plate with a height h_0 of several micrometers (h_0 is the height when the two surfaces are fully aligned). Below the shear band, the MR fluid behaves like a solid material. For shear nonparallel plates, the geometry relation $h(\rho, \theta, \varphi) = h_0 + \Delta h \left(1 - \frac{\rho}{D} (\cos(\theta - \varphi) + \cos\theta)\right)$ can be obtained, where ρ, θ is the coordinate parameter, φ is the rotation angle, $\Delta h = D \tan \alpha$ and is the maximum amplitude of the oscillation in local gap height as the tool rotates through one full turn. At a given φ , the element $dA = \rho d\rho d\theta$ bears a local normal force $dF = N_d/2dA = (N_{ds} + K\omega\rho/h(\rho, \theta, \varphi))\rho d\rho d\theta/2$. Integration of dA over the azimuthal and radial coordinates gives the total normal force on the tool,

$$F_N = \frac{1}{2} \int_0^{2\pi} \int_0^R \left(N_{ds} + \frac{K\omega\rho}{h_0 + \Delta h \left(1 - \frac{\rho}{D} (\cos(\theta - \varphi) + \cos\theta)\right)} \right) \rho d\rho d\theta$$

$$= \frac{1}{2} N_d \pi R^2 + \frac{K\omega}{2h_0} \int_0^{2\pi} \int_0^R \left(\frac{\rho^2}{1 + \varepsilon \left(1 - \frac{\rho}{D} (\cos(\theta - \varphi) + \cos\theta)\right)} \right) d\rho d\theta \quad (1)$$

Where $\varepsilon = \Delta h/h_0$, and this expression is valid for steady state shearing after the sample yielded and shows sinusoidal variations in $F_N(\varphi)$.

The parameters of MR fluid at 10 s^{-1} and 0.48 T were substituted to expression (1) and the relationship between normal forces and the rotation angle was shown in Fig. 4. This model fitting is semi-empirical because the tilted angle and the shear band are unknown, so the value ε is unknown and it is supposed to be a unit (the tilted angle is on the order of 10^{-4} degrees and the shear band is on the order of μm). Based on the above calculation, it can be seen that an obvious oscillatory normal force is obtained in our system. The peak–peak oscillatory normal forces increase with the increase in rotation angle. Under a small rotation angle, the generated oscillatory normal force is small. When the rotation angle is increased, the oscillatory normal force becomes more obvious. Integrating the expression (1) for different ε , it is found that the maximum oscillatory normal force increases with the parameter ε . Even if the tilted angle is very small the oscillatory normal forces of the MR fluid under steady shear will also exist. In practice, the nonparallelism of the plates cannot be eliminated from the testing setup and the oscillatory normal forces always exist. However, they can be weakened by making the plates more parallel.

3.2 Oscillatory normal force under oscillatory shear

The oscillatory normal forces of the MR fluid under oscillatory shear were also investigated. It is found that in the nonlinear viscoelastic region (strain amplitude > 0.1 – 0.5%), it can be obtained from a plot between the storage modulus and strain

amplitude of MR fluid, as shown in Fig. S5, ESI†), the normal forces oscillate with the testing time (Fig. 5). The applied strain was sinusoidal and its amplitude is 10% . At a frequency of 0.1 Hz (Fig. 5 (a)) the normal forces increase with the magnetic field. Under a stable field, the normal forces fluctuate in a period the same as that of the applied strain. In addition, similar oscillatory normal forces are found under different frequencies (Fig. 5 (b)). It can be found that the peak-peak amplitudes of oscillation normal forces decrease with increasing frequency. Similar to steady shear, the oscillatory normal forces have always existed under different concentrations, gap distances, and directions of the magnetic field.

The peak–peak amplitudes of oscillation normal forces of 30% MR fluids can reach as high as 3 N (10% of total normal forces), which is much larger than that under steady shear. Under this condition the oscillatory angle is so small (0.01 radian) that the oscillatory normal forces coming from the misalignment of plates are negligible. Therefore, the oscillatory normal forces under oscillatory shear does not come from misalignment of the plates and there must be another reason causing the oscillatory normal forces.

As the accurate constitutive model for the MR fluid under oscillatory shear is scarce, dynamic simulation is a better way to explain this phenomenon. Three dimensional dynamic simulations of MR fluids were carried out following the method developed by Klingerberg and co-workers.^{18–20} Simulations are performed in a periodic cell of dimensions $(L_x, L_y, L_z) = (10\sigma, 10\sigma, 10\sigma)$. The MR fluid is modeled as a suspension of N buoyant inertia-less particles in a Newtonian fluid with viscosity η and the relative magnetic permeability μ_r . The particles are monodisperse with a diameter σ and relative magnetic permeability μ_p (excluding magnetization saturation). Neglecting Brownian effects, forces here include the field-included magnetostatic pair interaction forces \mathbf{F}_{ij}^m (point dipole approximation), particles and particles short-range repulsive forces $\mathbf{F}_{ij}^{\text{rep}}$, particles and wall repulsive forces $\mathbf{F}_i^{\text{wall}}$ and hydrodynamic forces \mathbf{F}_i^h . For the particle i and j , the magnetostatic force on particle i due to particle j at the relative location (r_{ij}, θ_{ij}) is $\mathbf{F}_{ij}^m = F_0 \left(\frac{\sigma}{r_{ij}}\right)^4 \left[(3 \cos^2 \theta_{ij} - 1) \hat{\mathbf{r}} + \sin(2\theta_{ij}) \hat{\boldsymbol{\theta}} \right]$, where $F_0 = \frac{3}{16} \pi \mu_0 \mu_r \sigma^2 \beta^2 H_0^2$ is the magnetic field dependent constant; $\hat{\mathbf{r}}$ and $\hat{\boldsymbol{\theta}}$ are the unit vectors parallel and perpendicular to the line joining the pair of particles, respectively; H_0 is the applied magnetic field and μ_0 is the vacuum permeability. Short-range repulsive forces to prevent particles from overlapping are introduced as $\mathbf{F}_{ij}^{\text{rep}} = -2F_0 \left(\frac{\sigma}{r_{ij}}\right)^4 \exp[-100(r_{ij}/\sigma - 1)] \hat{\mathbf{r}}$. Similar expressions are employed for interactions between particles and bounding surfaces:

$$\mathbf{F}_i^{\text{wall}} = 2F_0 \left(\frac{\sigma}{\frac{1}{2}L_z + z_i}\right)^4 \exp\left\{-100\left[\left(\frac{1}{2}L_z + z_i\right)/\sigma - 0.5\right]\right\} \hat{\mathbf{z}}$$

$$- 2F_0 \left(\frac{\sigma}{\frac{1}{2}L_z - z_i}\right)^4 \exp\left\{-100\left[\left(\frac{1}{2}L_z - z_i\right)/\sigma - 0.5\right]\right\} \hat{\mathbf{z}}$$

The particles are also subjected to a drag viscous force. The hydrodynamic force on particle i is given by $\mathbf{F}_i^h = -3\pi\eta\sigma\left(\frac{d\mathbf{r}_i}{dt} - \mathbf{U}_f^\infty\right)$ in the free draining approximation, where \mathbf{r}_i and z_i are the coordinates of the particle i . \mathbf{U}_f^∞ stands for the ambient viscous fluid velocity at the center of particle i . The equation of motion in a dimensionless form for sphere i would reduce to

$$\frac{d\mathbf{r}_i^*}{dt} = \sum_{j \neq i} \mathbf{F}_{ij}^{m*} + \sum_{j \neq i} \mathbf{F}_{ij}^{\text{rep}*} + \sum \mathbf{F}_i^{\text{wall}*} + \mathbf{U}_f^{\infty*}(\mathbf{r}_i^*) \quad (2)$$

where the asterisks denote dimensionless quantities. The length, force, and time scales are given by

$$l_s = \sigma, F_s = F_0, t_s = 3\pi\eta\sigma^2/F_0$$

Two step simulations are made. Firstly, the $N = 572$ randomly dispersed particles are located in the box. The two wall are stationary and $\mathbf{U}_f^\infty(\mathbf{r}_i^*) = 0$. After certain steps, the steady chains or columns of particles will be generated in the box. Secondly, the oscillatory shear flow is applied on the generated structure. That is, a local shear strain $\gamma(t^*) = \gamma_0 \sin(\omega^* t^*)$ is added on the top wall while the lower one keeps stationary. Then the ambient fluid velocity is given by $\mathbf{U}_f^\infty(\mathbf{r}_i^*) = \omega^* \gamma_0 (z_i^* + L_z^*/2) \cos(\omega^* t^*) \mathbf{e}_x$. The dimensionless frequency is $\omega^* = \omega 16\eta/\mu_0\mu_f\beta^2 H_0$. Then, the sticking condition is applied, thus eqn (2) governs the motion of particles not near the wall; near the wall (the particle surface is within a distance δ_w of the wall) assumes that the lateral velocity of the particle is equal to the velocity of the wall and the z component of the motion is unaffected. So the equation can be rewritten as

$$\frac{dx_i^*}{dt^*} = u_{\text{wall}}^* \quad (3)$$

$$\frac{dy_i^*}{dt^*} = 0 \quad (4)$$

$$\frac{dz_i^*}{dt^*} = \sum_{i \neq j} F_{z,ij}^{m*} + \sum_{i \neq j} F_{z,ij}^{\text{rep}*} + \sum F_{z,i}^{\text{wall}*} \quad (5)$$

and the wall velocity u_{wall}^* is given as $u_{\text{wall}}^* = \dot{\gamma}^* L_z^*$ for the top wall and $u_{\text{wall}}^* = 0$ for the bottom wall. The equations of motion were integrated numerically using an explicit Euler method with a dimensionless $\Delta t^* = 2 \times 10^{-4}$. The walls are placed at $z^* = \pm l_z/2 = L_z/2\sigma$ and periodic boundaries are located at $x^* = \pm l_x/2$ and $y^* = \pm l_y/2$. Furthermore, the overall dimensionless average stress in the system, especially the normal stress $\bar{\sigma}_{zz}^*$ along the magnetic field were calculated by²¹

$$\bar{\sigma}_{zz}^* = \frac{1}{V^*} \sum_{k=1}^{n-1} \sum_{i \leq k} \sum_{j > k} F_{ij}^* \Delta r_k^* \quad (6)$$

where F_{ij}^* is the interaction force between different layers; Δr_k^* is the interval between the layers and n is the number of layers.

The simulated normal stress of the MR fluid is given in Fig. 6. The applied strain amplitude γ_0 is 10% and three dimensionless angular frequencies 0.01, 0.1, 1 are calculated. Obviously the oscillatory normal stresses occur. Fig. 7 shows the relative

microstructure revolution of MR fluid under oscillatory shear. Fig. 7 (a) is the initial structure that the particles are randomly dispersed in the dimensionless box. After certain steps (10^6) the steady chains or columns are formed in the fluid under the magnetic field (Fig. 7 (b)). The chains or columns are the origin of the normal forces which push the plate apart. The formed steady structure is then used as the beginning structure under oscillatory shear. The red arrow indicates the direction of chains. Fig. 7(c)–(f) shows the structure revolution of MR fluid in a cycle and similar can be found in other cycles (not shown here for brevity). It can be seen that the arrow moves with the motion of the top plate. These recycle structures lead to the oscillation of the normal force under oscillatory shear. Of course the chains or columns rupture and rebuild in this process which make the simulated normal stress rough.

The simulated peak–peak normal stress increases with the increased frequency which is opposite to the experimental tests. The difference comes from the sticking boundary condition in simulation. In the experiment, slipping between the iron particle and the plate existed. With increasing frequency, the slipping becomes more significant, and the peak–peak normal force decreases. However, in simulation the sticking boundary condition is applied and the iron particle will follow the plate. With increasing frequency, the shear rate increases and the peak–peak normal force increases. Besides, the peak–peak value can reach 20% of the total normal stress and that is twice of that by the experimental investigation. These may also originate from the sticking boundary condition in simulation. In experimental testing the particles will slip on the wall which would weaken the pushing effect on the wall. Furthermore, the inhomogeneity of the applied field in testing will also affect the normal forces.^{17,22} The simulation normal stress is smaller than the experimental value because of the point-dipole approximate mode. However, this does not affect the results in nature.

3.3 Comparison between the two oscillatory normal forces

The microstructure of MR fluids under steady shear with ideal parallel plates must have a stable structure. In theory, the normal forces under steady shear with ideal plates should have a constant value. However, the oscillatory normal forces under steady shear do exist as a result of the nonparallelism effect of the realistic plates. This oscillatory normal force can't be eliminated but only weakened with more parallel plates (reduce the parameter ε). Sometimes it would affect the experimental accuracy to a large degree.

However, the oscillatory normal forces under oscillatory shear differ from that under steady shear. Under small amplitude oscillatory shear, the misalignment effect of the plates on the normal forces is very small. The oscillatory normal forces mainly arise from the microstructure revolution of MR fluids under oscillatory shear. They are the physical manifestation of MR fluids. It will always exist in the oscillatory shear. As the peak–peak oscillatory normal forces under steady shear increase with the rotation angle (Fig. 4), if a larger oscillatory shear amplitude is applied, the oscillatory normal force arise from misalignment of the plates can't be neglected. Then the oscillatory normal forces under oscillatory shear come from both the misalignment of the plates and the microstructure revolution of MR fluids.

4. Conclusions

In this study, the two ways to generate oscillatory normal forces of MR fluids were investigated and compared by a plate–plate magneto-rheometer. For 30% MR fluids, the peak–peak amplitude oscillatory normal forces under steady shear are about 0.4 N (2% of total normal forces), which are from misalignment of the plates. The peak–peak amplitude oscillatory normal forces under oscillatory shear are about 3 N (10% of total normal forces), which arise from both the nonparallelism effect of the plates and the microstructure revolution of MR fluids. A dynamic simulation is used to calculate the normal stress of MR fluids under oscillatory shear. All these will help understand the normal behavior of MR fluids and remind the possible error of normal forces of MR fluids in testing.

Acknowledgements

Financial supports from the National Natural Science Foundation of China (Grant Nos. 11125210, 11072234, 11102202), the National Basic Research Program of China (973 Program, Grant No. 2012CB937500) and the Specialized Research Fund for the Doctoral Program of Higher Education of China (Project No.20093402110010) are gratefully acknowledged.

References

- 1 J. de Vicente, D. J. Klingenberg and R. Hidalgo-Alvarez, *Soft Matter*, 2011, **7**, 3701–3710.
- 2 D. J. Klingenberg, *AIChE J.*, 2001, **47**, 246–249.
- 3 W. Q. Jiang, Y. L. Zhang, S. H. Xuan, C. Y. Guo and X. L. Gong, *J. Magn. Magn. Mater.*, 2011, **323**, 3246–3250.
- 4 X. Z. Zhang, W. H. Li and X. L. Gong, *Smart Mater. Struct.*, 2010, **19**, 125012.
- 5 O. Ashour, C. A. Rogers and W. Kordonsky, *J. Intell. Mater. Syst. Struct.*, 1996, **7**, 123–130.
- 6 J. D. Carlson, D. M. Catanzarite and St K. A. Clair, *Int. J. Mod. Phys. B*, 1996, **10**, 2857–2865.
- 7 J. de Vicente, F. González-Cabellero, G. Bossis and O. Volkova, *J. Rheol.*, 2002, **46**, 1295–1303.
- 8 Y. M. Shkel and D. J. Klingenberg, *Proceedings of the 7th International Conference on Electro-rheological Fluids, Magnetorheological Suspensions*, 1999.
- 9 H. See and R. Tanner, *Rheol. Acta*, 2003, **42**, 166–170.
- 10 H. M. Laun, C. Gabriel and G. Schmidt, *J. Non-Newtonian Fluid Mech.*, 2008, **148**, 47–56.
- 11 M. T. López-López, P. Kuzhir, J. D. G. Durán and G. Bossis, *J. Rheol.*, 2010, **54**, 1119–1136.
- 12 Y. T. Chan, P. Wong, K. P. Liu and W. Bullough, *J. Intell. Mater. Syst. Struct.*, 2011, **22**, 551–560.
- 13 J. L. Jiang, Y. Tian, D. X. Ren and Y. G. Meng, *Smart Mater. Struct.*, 2011, **20**, 085012.
- 14 C. Y. Guo, X. L. Gong, S. H. Xuan, L. H. Zong and C. Peng, *J. Magn. Magn. Mater.*, 2012, **324**, 1218–1224.
- 15 C. S. Orellana, J. He and H. M. Jaeger, *Soft Matter*, 2011, **7**, 8023.
- 16 E. Andablo-Reyes, J. de Vicente and R. Hidalgo-Alvarez, *J. Rheol.*, 2011, **55**, 981–985.
- 17 E. Andablo-Reyes, R. Hidalgo-Alvarez and J. de Vicente, *Soft Matter*, 2011, **7**, 880–883.
- 18 D. J. Klingenberg, F. van Swol and C. F. Zukoski, *J. Chem. Phys.*, 1989, **91**, 7888–7895.
- 19 D. J. Klingenberg, *J. Rheol.*, 1993, **37**, 199–214.
- 20 J. C. Ulicny, K. S. Snavely, M. A. Golden and D. J. Klingenberg, *Appl. Phys. Lett.*, 2010, **96**, 231903.
- 21 Z. H. Sun, X. X. Wang, A. K. Song and H. A. Wu, *Modell. Simul. Mater. Sci. Eng.*, 2006, **14**, 423–431.
- 22 H. M. Laun, G. Schmidt, C. Gabriel and C. Kieburg, *Rheol. Acta*, 2008, **47**, 1049–1059.